

Shake Table Testing of Bidirectional Ductile Diaphragms with Buckling-Restrained Braces in V-shaped configuration

Homero Carrion-Cabrera^{a,*}, Michel Bruneau^{b,2}

^a Kiewit Infrastructure Engineering, Bellevue, WA 98004, USA

^b Dept. of Civil Structural and Environmental Engineering, University at Buffalo, Buffalo, NY 14260, USA

ARTICLE INFO

Keywords:

Buckling Restrained Braces
Multi-Span Bridges
Seismic Performance
Temperature effects
Shake table

ABSTRACT

The Bidirectional Ductile Diaphragm concept relies on Buckling Restrained Braces (BRBs) used at ends of spans in common multi-span bridges to provide seismic resilient damage-free bridges at low cost, while minimizing displacement demands to levels that can be easily accommodated by conventional expansion joints. This paper reports on the results of a shake-table testing program of Bidirectional Ductile Diaphragms designed with Buckling Restrained Braces (BRBs) deployed in a V-shaped layout. A single span taken from a scaled straight bridge with no skew, simply supported on slider bearings, and BRBs end connection details was subjected to: (1) earthquakes scaled to match the design level; (2) BRB deformation demands corresponding to 75 years of cycles of bridge thermal expansions, and; (3) earthquake scaled to levels exceeding the design level such as to bring the BRB to fracture upon repeated cycles of large inelastic deformations at extreme ductility demands. Results demonstrate that bridges using the bidirectional ductile end diaphragm concept with BRBs in a V-shaped configuration can develop a stable hysteretic response, with inelastic deformations concentrated in the BRBs. These bridges would experience no loss of functionality following an earthquake, resulting in fully resilient bridges that remain in service throughout and after the earthquake.

1. Introduction

Buckling restrained braces (BRB) are special braces capable to yield in axial tension and compression. They can develop large ductility, produce stable hysteretic behavior, and dissipate large amounts of seismic energy – capabilities that are valuable in seismic resisting structures. Initially, these elements were first introduced in buildings in Japan in 1987, in the USA in 1999 [2], and in many other countries since. They are nowadays widely used and design requirements for buckling restrained braced frames are specified by the AISC Seismic Provisions for Structural Steel Buildings [3]. Given that all the yielding in a BRB happens inside its casing, to help structural engineers determine if BRBs should be replaced following an earthquake, some manufacturers have also integrated into their BRBs displacement transducers capable of recording the history of cyclic deformations of the brace yielding core over time; this information can then be used to calculate the BRB remaining fatigue life and avoid premature replacement after major earthquakes and/or several years of services. In bridges, there

have been much fewer applications to date. Examples include the Vincent Thomas Bridge [13,14] and the Minato bridge [15] which were retrofitted with BRBs.

Yet, BRBs are well suited to be used in a bi-directional ductile diaphragm concept. A ductile end diaphragm consists of hysteretic devices (or “structural fuses”) implemented in the diaphragms located at the ends of spans. These ductile end diaphragms are intended to dissipate seismic energy and prevent damage in the substructure by limiting the magnitude of transmitted forces. The concept was initially developed and tested with various hysteretic devices for seismic forces in the transverse direction by Zahrai and Bruneau [22] and a design procedure provided by Alfawakhiri and Bruneau [4] has been implemented in AASHTO [1]. Further shake table studies verified the concept by exciting, in their transverse direction, scaled bridges having BRBs as fuse elements at their end diaphragms [6]. Later, the concept was expanded to bidirectional seismic forces for bridges with stiff structures [11,21] and a design procedure was also provided for the case of rigid piers. The concept of bidirectional ductile end diaphragm emphasizes the ability to

* Corresponding author.

E-mail addresses: homerofe@buffalo.edu (H. Carrion-Cabrera), bruneau@buffalo.edu (M. Bruneau).

¹ ORCID: 0000-0001-6335-2060.

² ORCID: 0000-0003-1170-468X.

dissipate energy under both longitudinal and transverse seismic excitations. The advantage of this system is the restriction of displacements between spans, which can be accommodated with low-cost expansion joints, and the prevention of damage to substructural elements when bridges are seismically excited in both horizontal directions, assuming that all other parts or components of the bridge are designed to develop the BRB capacity (per capacity design principles). This results in seismic resilient damage-free bridges that are fully operational following an earthquake, therefore meeting resilience objectives [5].

Currently, if wishing to use BRBs to implement a bidirectional diaphragm strategy, AASHTO provides simple equations that could be used for the transverse direction, but there is no verified procedure available other than performing Non-Linear Response History Analysis (NL-RHA) to design BRBs in the longitudinal direction [7]. To remedy this, Carrion-Cabrera and Bruneau [8,10] developed a Multimodal procedure and an Equivalent Lateral Force (ELF) procedure for this purpose and validated their effectiveness analytically for simply-supported multi-span bridges having 2 to 11 spans, with spans supported by bidirectional sliding bearings.

An experimental project was developed and conducted by the authors to validate the concept of ductile diaphragms using BRBs in such bridges, designed per the above procedures. This experimental work involved conducting shake-table testing of a scaled bridge span on slider bearings, and BRBs end connection details. The two shake tables at the University at Buffalo's (UB) Structural Engineering and Earthquake Simulation Laboratory (SEESL) were used working asynchronously for this purpose, with each end of the tested span supported on a shake table. A special V-braced BRB configuration was investigated as part of this project, and subjected to: (1) earthquakes scaled to match the design level; (2) BRB deformation demands corresponding to 75 years of cycles of bridge thermal expansions (because longitudinal BRBs that connect spans to their abutment and piers span across expansion joints), and: (3) earthquake scaled to levels exceeding the design level such as to bring the BRB to fracture upon repeated cycles of large inelastic deformations at extreme ductility demands. This special V-braced configuration was represented with two sets of BRBs, each set having different BRB connections. The advantage of this configuration is that BRBs are protected from possible vehicle impact since they are located between the girders (contrary to the case where BRBs would be connected to the underside of the bridge girders), and that larger yield displacements can be obtained in the system of BRBs that reduces seismic forces than if the BRBs used were oriented in the directions parallel and perpendicular to the span. This paper presents the results of this experimental program.

2. Equivalent lateral force design equation

In the longitudinal direction, the ELF procedure proposed by Carrion-Cabrera and Bruneau [10] was used. For this BRB configuration, the steps of that design procedure are as follow:

- 1) Define the geometry of the BRBs in a V-shape configuration (i.e., BRBs length, and their inclination angles with the vertical and horizontal planes).
- 2) From the V-shape geometry, calculate the horizontal yield deformation of the group of BRBs in V-shape configuration. As a rule of thumb, the BRB length should be larger than 6 % the span length [21].
- 3) Define the target ductility of the brace, μ_{ig} , and check that the corresponding local ductility of the core is less than 10.
- 4) Calculate the BRB target deformation corresponding to the values in Step 2.
- 5) Calculate the seismic mass of the span.
- 6) Analyze one span as a SDOF system and find the period to reach the system target deformation using the following steps.

a. Calculate the inelastic spectral displacement as:

$$S_d(T) = R_d(T) \cdot g \cdot Sa(T) \cdot \left(\frac{T}{2\pi}\right)^2 = \frac{\mu_{ig}}{R(T)} \cdot g \cdot Sa(T) \cdot \left(\frac{T}{2\pi}\right)^2 \quad (1)$$

where $R(T)$ is given by Eq. (16) and assuming $\gamma_\mu = 1$, and R_d is the displacement amplification factor for short period system, $Sa(T)$ is the design spectrum, and g is the gravity acceleration

- b. Calculate the period of the SDOF, or also called the minimum period of the structure T_{min} . The period of the SDOF can be obtained by solving the following equation:

$$\Delta_y \cdot \mu_{ig} = S_d(T_{min}) = \frac{\mu_{ig}}{R(T)} \cdot g \cdot Sa(T) \cdot \left(\frac{T}{2\pi}\right)^2 \quad (2)$$

$$\Delta_y = \frac{g \cdot Sa(T_{min})}{R(T_{min})} \cdot \left(\frac{T_{min}}{2\pi}\right)^2 \quad (3)$$

The solution could be solved graphically by drawing the inelastic displacement spectrum and locating the period for which the system target deformation is obtained.

- 7) Calculate T_p , which is the period of one pier modeled as a SDOF with stiffness equal to the pier stiffness of the bridge and mass equal to the pier tributary mass in the bridge.

$$T_p = 2\pi \sqrt{\frac{M}{K_p}} \quad (4)$$

- 8) Calculate auxiliary parameters defined as:

$$\gamma = \frac{T_p}{T_{min}} \quad (5)$$

$$\lambda = 1 - \frac{8}{\gamma^2 + 8} \quad (6)$$

$$\eta = \frac{T_1}{T_{min}} = 1 + 0.4 \cdot \lambda \cdot N_{span} \quad (7)$$

- 9) Calculate the period of the structure (T) in the longitudinal direction

$$T_1 = \eta \cdot T_{min} \quad (8)$$

- 10) Calculate the mode shape

$$\phi(x, k_1, k_2) = 1 + y(x, k_1) - y(x, k_2) \quad (9)$$

$$x = 1 - 2 \frac{i - 1}{N_{span} - 1} \quad (10)$$

$$y(x, k) = 1.0 - \left(0.60 + \frac{u_{ig}}{100}\right) \left[1 - \left(1 - \frac{|x|^k}{1.1}\right)^k\right] \quad (11)$$

$$k_1 = 4 \cdot \lambda \leq 0.15 \cdot (10 + \mu_{ig}) \cdot (1 - 0.7^{N_{mas}-2}) \quad (12)$$

$$k_2 = 0.06(\gamma - 1) > 0 \quad (13)$$

- 11) Calculate the reduction factor for the bridge

$$1.0 \leq \alpha_\mu = 0.06\mu_{SDOF} + 0.7 \leq 1.3(14)$$

$$\gamma_\mu = 2 \cdot \eta - 1 \leq 2 \quad (15)$$

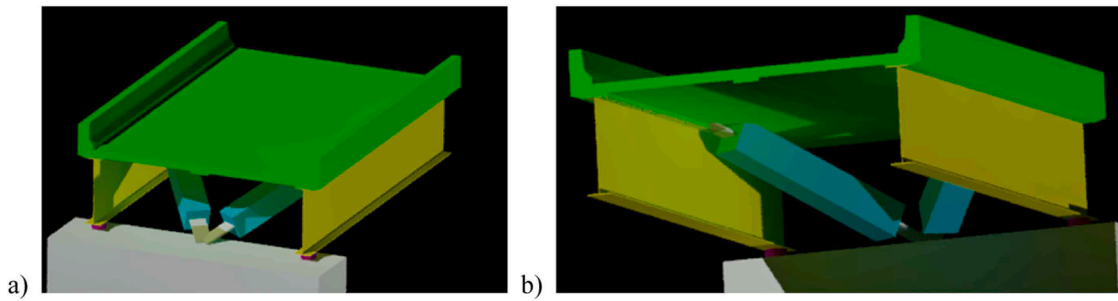


Fig. 1. BRB Configuration: a) end view; b) view from below deck.

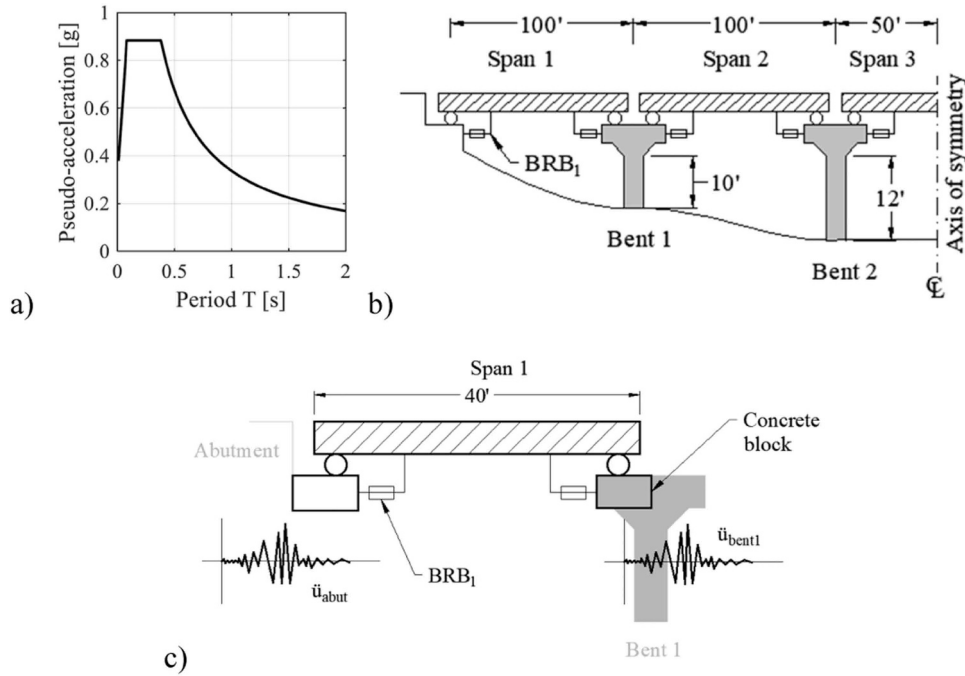


Fig. 2. Prototype: a) design spectrum, b) scheme in the longitudinal direction, c) model of the shake table test.

$$R(T_1) = \begin{cases} \left(\frac{\mu_{rg}}{\alpha_\mu \gamma_\mu} - 1 \right) \frac{T_1}{1.25T_s} + 1 & \text{if } T_1 < 1.25T_s \\ \frac{\mu_{rg}}{\alpha_\mu \gamma_\mu} & \text{otherwise} \end{cases} \quad (16)$$

12) Calculate the equivalent lateral force

$$F_i = \frac{WSa(T)}{R} \frac{m_i \phi(x_i)}{\sum_{j=1}^n m_j \phi(x_j)} \quad (17)$$

This proposed simplified design ELF procedure can be used to obtain BRB target ductility demands ranging from 5 and 10 (depending on the R-factor used). The displacement demands in piers and expansion joints can be limited by an adequate selection of the BRB target ductility and BRB yield deformation.

3. Specimen design and fabrication

For the shake table experiments, a 5-span regular span bridge having 100 ft simply supported spans was designed as a prototype from which the span connecting to the abutment and a bent was selected to design a representative specimen scaled 1/2.5 for the shake table experiments.

The configuration recommended for testing has the BRBs neither aligned with the longitudinal direction nor with the transverse direction, but rather installed at an angle with both of these orthogonal axes. An example of this configuration is shown in Fig. 1 where the two BRBs are connected to a common point at the substructure and the BRBs are connected to the top flange (or close to it) of different girders. In this case, both BRBs work together to simultaneously provide strength in the longitudinal and transverse direction. Although the above simplified ELF procedure was developed for BRBs working independently in each direction, for this configuration, this procedure was also used to design for the seismic motions in the longitudinal direction and displacement-based design was used to design for the component in the transverse direction. The difference in how the design procedures were applied here is that BRBs were designed to reach a target ductility in the transverse direction equal to 70 % of the one that would have been predicted assuming response purely in the transverse direction. Furthermore, the design spectrum for Memphis, Tennessee, was selected for design for consistency with previous work [20,7,8], and it is shown in Fig. 2a. The design in the longitudinal and transverse direction resulted in two different sets of BRB areas at each end of the span, the larger resulting BRB area at the end of each span was used as the design value of the BRBs there. As for the connections, they are all subjected to rotations about two orthogonal axes that results from displacements in the longitudinal and transverse directions; they were therefore detailed

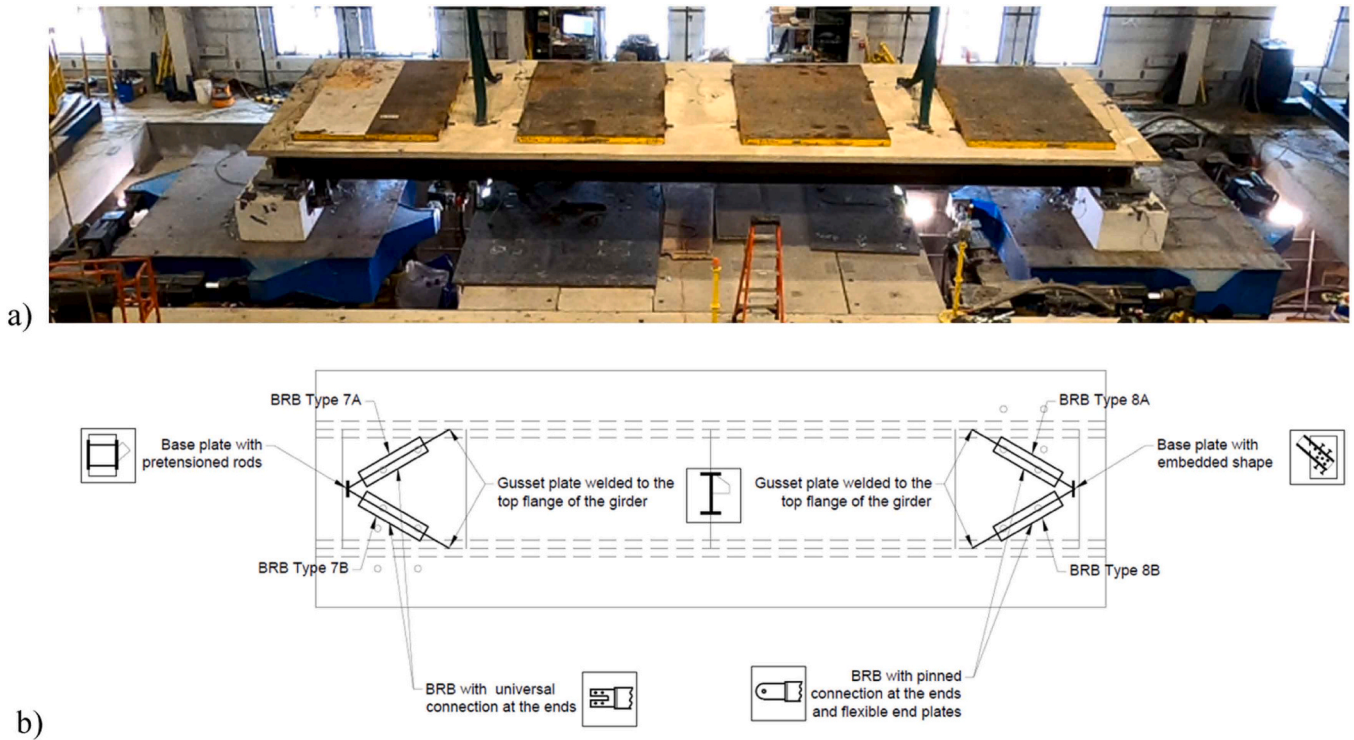


Fig. 3. Experiment set-up for Set 1: a) top view, b) sketch of the location of BRBs and different type of connections used.

to accommodate these displacements.

The specimen was designed to represent the span close to the abutment of a prototype simply supported 5-span bridge. The prototype and the testing specimen are shown in Fig. 2b. More information can be obtained in Carrion-Cabrera and Bruneau [9].

Beyond the BRBs expected to act as fuse elements dissipating seismic energy, to meet the objective of avoiding damage in the remaining structure, all other components were designed based on plastic analysis and capacity design principles considering that BRBs reach their maximum probable force. This included connections between BRBs and base plate, connection between base plates to foundation, connection between BRB to girders, bearings and connection to foundation and girder, concrete foundation, and connection of foundation to shake table.

Due to the BRBs small length and strength required to fit the scaled specimen, two BRB prototypes were tested following the ANSI/AISC 341 (2022) procedure to verify that they would develop adequate hysteretic behavior and maximum ductility. This process also allowed to establish the strain hardening parameters needed for the capacity design and to finalize the design of the specimen.

Likewise, the slider bearings used to support the specimen were subject to quasi-static testing to establish their friction coefficient. It was found that the sliding force was approximately 1.5 % of the strength of

the BRBs. The bearings were connected on top of concrete blocks representing a bridge abutment at one end, and a pier cap at the other end. Those blocks were in-turn connected to their respective shake table. A total of 156 accelerometers, string potentiometers, linear potentiometers, and strain gauges were installed to record the dynamic response of the specimen, and (most importantly) to track behavior of each BRB while being tested on the shake table. The added mass plates were attached to the top of the deck to respect scale-testing similitude laws.

4. BRB configuration and testing protocol

The configuration considered here has all BRBs oriented at an angle of 30 degrees from the longitudinal axis of the bridge and 30 degrees with the horizontal plane, at each end of the bridge, for a total of four BRBs in each set, as shown in Fig. 3. Based on the stiffnesses of the structure in each direction, all BRBs were originally designed to have the same yield strength (note that piers in the prototype were relatively rigid in the transverse direction and flexibles in the longitudinal direction). However, the received BRBs had different yield strengths (as described earlier): in Set 1, two BRBs had a steel core with a yield strength of 38.1 ksi, and two with 52.1 ksi; in BRBs Set 2, all BRBs had a steel core with a yield strength of 52.1 ksi. The properties of the BRBs are listed in Table 1. Therefore, for Set 1, at each end of the deck, one BRB of each

Table 1
Properties of received BRBs.

BRB type	BRB set	K_{BRB} [Kip/in]	Core Area [in ²]	Yielding core Length [in]	Core yielding stress [ksi]	Yielding Force [kips]	$\Delta_{y_{global}}$ [in]	$\Delta_{y_{local}}$ [in]
7a	1	457	0.5	23.65	38.1	19.1	0.042	0.031
7b	1	457	0.5	23.65	52.9	26.5	0.058	0.043
8a	1	360	0.5	24.7	38.1	19.1	0.053	0.032
8b	1	360	0.5	24.7	52.9	26.5	0.073	0.045
9b	2	339	0.5	25.4	52.9	26.5	0.078	0.046

NOTE: K_{BRB} is the BRB stiffness, $\Delta_{y_{global}}$ is the global BRB yield deformation, and $\Delta_{y_{local}}$ is the BRB core yield deformation.

Table 2
Ground motions used in shake testing program.

Group	Ground motion name	Data source
Spectral matched motions	Imperial Valley	PEER [17] ground motion # 169
	Chi-Chi	PEER ground motion # 1244
	Manjin, Iran Synthetic	PEER ground motion # 1633 Created using SeismoArtif [18]
Ground motions scaled beyond design level	Northridge – FF	PEER ground motion # 953
	El Centro	PEER ground motion # 6
	Kobe – Pulse	PEER ground motion # 1114
	Kobe – FF	PEER ground motion # 1116
Motions assuming rigid piers	Puebla – Mexico	Mexico, Roma Norte 2017, CIRES [12]
	Pedernales – Ecuador	Ecuador, Portoviejo 2016, RENAC [19]

strength were used. They were located such that the weakest BRBs were connected to the north girder and the strongest BRBs were connected to the south girder, as shown in Fig. 3. For Set 2, all four BRBs were identical.

The design spectrum was based on force demands in BRBs calculated with the defined design methodology. The design demands were therefore modified to match the properties of the received BRBs. Note that in this configuration, the response in the longitudinal direction controlled the design in BRBs connected to abutments, and the transverse direction controlled the design in BRBs connected to piers. The period of the structure was 0.216 s and 0.162 s in the longitudinal and transverse directions, respectively.

The testing protocol was defined as a series of steps followed during testing of the specimen. The word “steps” refers to the different stages of testing. The specimen was subjected to: (1) earthquakes scaled to match the design level; (2) BRB deformation demands corresponding to 75

years of cycles of bridge thermal expansions, and: (3) earthquake scaled to levels exceeding the design level such as to bring the BRB to fracture upon repeated cycles of large inelastic deformations at extreme ductility demands. During testing, one shake table represented the motion of the abutment while the other represented the motion of the top of the pier, as shown in Fig. 2c. All motions were obtained from a numerical model, to be able to represent the motion of the pier. The seed ground motions are presented in Table 2. Each history used during testing, even if it was not at the maximum scale expected to be used during testing, was considered as a different step.

5. Shake table testing

Fig. 4 shows the position of the BRBs in the bridge. Note that, for new construction, BRBs would be typically installed after the deck is cast, as done in the experiment. Once the BRBs were installed, all instruments were attached, and the bridge was ready to be tested. The test sequence was updated in real-time during execution of the testing program based on the observed behavior of the structure. The temperature sequence was the first applied, followed by ground motions histories. Note that the first group of ground motions were initially spectral matched to the design spectrum. If that group of ground motions was not able to fail a BRB, the test continued with a group of ground motions scaled beyond design level and finally with history of motions assuming rigid piers. During testing, a secondary amplitude scale was applied to all motions, as shown in Table 3, to obtain the largest possible demand in BRBs (based on numerical analysis).

6. Test results for BRBs Set 1

The temperature sequence was applied before any seismic motion because data reading from the BRBs during this test sequence can provide information about the yielding point of the members. During testing, upward bending of the deck was observed due to the uplifting forces introduced by BRBs in compression. This contributed to create

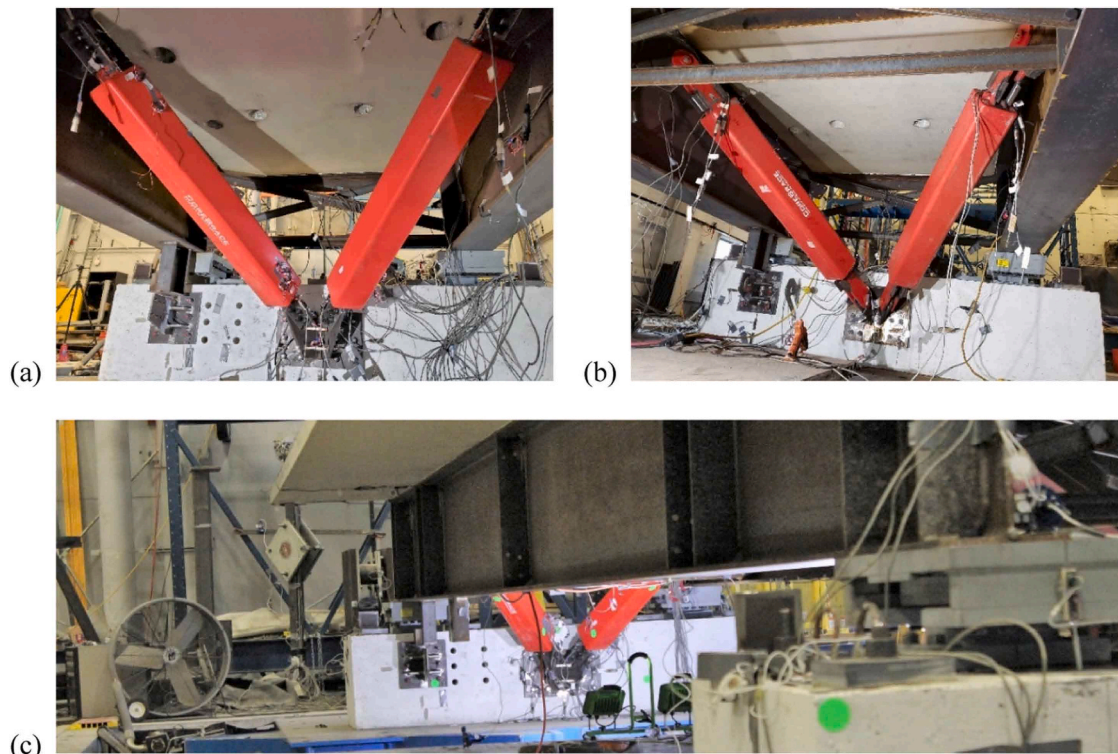


Fig. 4. Photos: a) BRBs west side, b) BRBs east side, c) side view of installed BRBs.

Table 3
Test sequence and summary of BRB demands for Set 1.

Step No.	Seismic Step No	Motion	Motion name	Scale [%]			Apparent core ductility demand				Fatigue				Cumulative inelastic deformation [Δ_y]			
				X	Y	Z	WN	WS	EN	ES	WN	WS	EN	ES	WN	WS	EN	ES
11		T2	Temp. 75 years	185	-	-	1.4	1.0	1.5	0.8	-	-	-	-	3	-	1	-
29	6	E01	Imperial Valley	100	100	-	5.7	4.1	6.6	1.3	3	1	1	-	88	12	24	-
41	9	E02	Chi-Chi	100	100	-	5.2	3.2	7.5	1.7	2	1	1	-	151	22	58	-
49	11	E03	Manjin, Iran	100	100	-	6.5	3.5	4.3	1.6	1	-	1	-	185	34	69	-
57	13	E04	Synthetic	100	100	-	6.5	3.6	6.3	2.4	2	2	1	1	265	58	90	1
61	14	E04	Synthetic	100	-	-	5.0	2.8	1.5	0.7	1	1	-	-	317	68	90	1
62	15	E04	Synthetic	-	100	-	2.9	1.5	6.1	2.4	-	1	1	-	321	68	108	2
63	16	E04	Synthetic	125	125	-	9.2	5.9	8.9	3.0	6	5	2	1	500	148	158	7
67	17	E01	Imperial Valley	125	125	-	12.0	8.2	10.4	3.1	5	4	4	1	658	206	227	12
71	18	E02	Chi-Chi	125	125	-	10.2	5.6	12.7	3.3	4	4	4	1	762	256	303	17
72	19	E03	Manjin, Iran	125	125	-	8.4	5.7	6.6	3.2	2	2	2	1	836	298	331	20
80		T2	Temp. 75 years	290	-	-	2.7	2.1	3.6	1.8	-	2	1	1	838	299	335	21
86	22	E11	Ecuador RP	100	-	-	9.5	6.5	8.5	4.5	2	3	1	1	911	342	380	37
87	23	E11	Ecuador RP	-	100	-	5.8	2.3	7.8	3.3	1	-	2	1	928	345	416	42
91	24	E11	Ecuador RP	100	100	-	19.7	7.5	9.6	7.6	7	2	3	4	1060	375	474	77
99	26	E05	El Centro	100	100	-	8.3	6.5	7.4	4.4	2	2	2	1	1108	400	508	91
104	28	E06	Northridge - FF	100	100	-	10.5	13.1	15.7	6.8	2	4	8	2	1167	442	630	117
112	30	E09	Mexico	100	100	-	10.8	7.0	16.5	3.7	7	4	6	2	1292	497	724	128
116	31	E09	Mexico	125	125	-	17.7	15.4	26.5	5.8	16	15	18	4	1545	636	907	166
120	32	E09	Mexico	125	-	-	11.1	6.2	3.8	1.8	4	4	-	-	1647	686	910	166
121	33	E09	Mexico	-	125	-	11.4	6.8	19.5	8.0	4	3	12	4	1734	730	1067	208
129	35	E08	Kobe - FF	100	100	-	28.9	4.8	8.4	6.3	7	1	2	2	1821	743	1100	222
134	37	E07	Kobe - Pulse	100	100	-	14.1	38.5	89.4	12.1	3	14	8	4	1863	815	1156	252
138		T1	Temp. 3 cycles	300	-	-	0.3	16.8	8.0	0.2	-	-	-	-	1863	815	1156	252
139		T1	Temp. 3 cycles	600	-	-	0.9	27.4	19.4	0.6	-	-	-	-	1863	815	1156	252

Note: WN = West north BRB, WS = West south BRB, EN = East north BRB, ES = East South BRB

Gray shaded = Elastic behavior
 Green shaded = Ductilities larger than 10 and lesser than 20
 Orange shaded = Ductilities larger than 20

Values in Italic and underlined = Values after failure (for comparison purposes only)
 Bolt values = Fracture

Table 4
Mean of deformation demands in BRBs in inches.

Description	BRB			
	WN	WS	EN	ES
Numerical result of the 4 spectrally matched motions	0.274	0.297	0.146	0.157
Experimental results with motions at 100 %	0.184	0.154	0.194	0.078
Experimental results with motions at 125 %	0.305	0.279	0.301	0.141
Ratio between experiment at 100 % to numerical	0.67	0.52	1.33	0.50
Ratio between experiment at 125 % to numerical	1.11	0.94	2.06	0.90

smaller than expected BRB deformation demands. Multiple 3-cycle sequences were used to adjust the scale of the displacement amplitude before running the 75-cycle sequence. After a more detailed check of the data obtained for the 75-cycle sequence, this configuration was retested under the temperature sequence a second time with a larger displacement amplitude after testing with the spectral matched motions was completed. Again, the new displacement magnitude was obtained through testing iterations using 3-cycle sequences.

During the testing with ground motions, due to the configuration of BRBs, uplift was experienced at the bearings several times. Uplifting was identified by the impact sounds that accompanied it (this was expected, and the bearings were designed to “catch” and restrain uplifting of the girder). Testing ended when two BRBs failed during the Kobe motion at Step 134: the strong BRB in the west side (West south) and the weak BRB in the east side (East north).

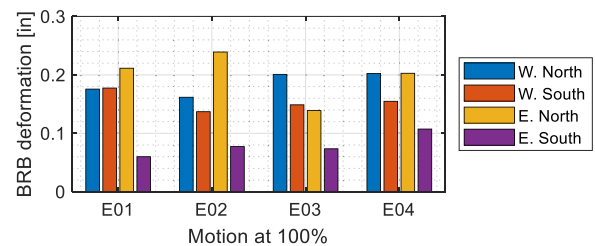


Fig. 5. BRB maximum deformation for spectral matched motions at 100 %.

6.1. BRB demands

For the configuration of BRBs used in this test, the demands cannot be decoupled in transverse and longitudinal directions. Instead, both BRBs works as a unity for motions in the transverse or longitudinal direction. Therefore, BRBs will have larger demands under bidirectional motions than only under individual unidirectional motions.

To compare results between motions, deformation demands were calculated as the relative demand with respect to the deformation at the start of the step, and are called “apparent deformations” here. The mean demands obtained from the numerical analysis for the BRBS are listed in Table 4 and a comparison of the BRBs deformation demands for each motion is shown in Fig. 5. From the table it is observed that, in most of the cases, the experimentally obtained demands were smaller than expected from numerical analysis. From the data in the table for motions at 100 % scaling, the mean experimental demands range from 0.50 to 1.33 of the numerical demands. Three of the four BRBs had less demand than obtained from the numeric model.

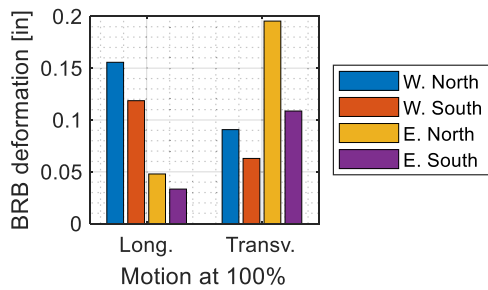


Fig. 6. BRB maximum deformation for spectral matched motions at 100 % and under unidirectional excitation of Motion E04.

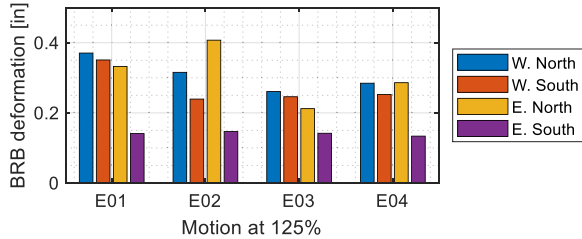


Fig. 7. BRB deformation for spectral matched motions at 125 %.

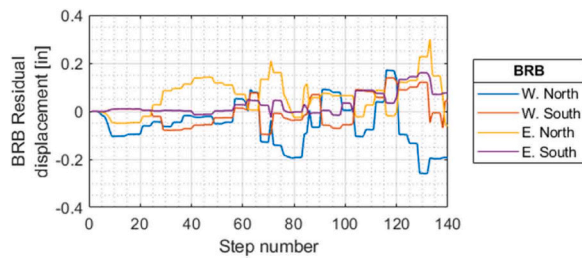


Fig. 8. BRB residual deformation.

One motion representing the design spectrum was also used to evaluate the specimen under unidirectional excitations. Demands obtained are shown in Fig. 6. Note that the BRBs connected to the west block (abutment) are the ones that experienced the larger demands under the uniaxial longitudinal motion while the BRBs connected to the east block (pier) are those that experienced the greater demands for the uniaxial transverse motion. This is similar to what was observed in design, where the longitudinal direction excitation controlled the design of the BRBs connected to the abutment and the transverse direction excitation controlled the design of the BRBs connected to piers. Comparing demands under unidirectional motions with demands under bidirectional motions (Fig. 5), shows that demands in BRBs connected to the west block (representing the abutment) were always smaller for unidirectional excitation than in the bidirectional case, and; for BRBs connected to the east block (representing the pier cap), demands under the unidirectional motion in the transverse direction was approximately equal to the demands under bidirectional motions.

To investigate the behavior to a larger demand than considered in design, the specimen was tested to 125 % of the design spectrum. The mean demands are listed in Table 4 and a comparison of the BRB deformation demands for each motion is shown in Fig. 7. From the data in the table for motions at 125 % scaling, it is observed that BRB mean demands range from 0.90 to 2.06 of the numerical demands (evidently, larger than demands for motions at 100 %).

A ductility demand was calculated for each ground motion test. The term “apparent” is used to calculate the BRB ductility demand with respect to its state at the beginning of a motion. As a simplification to

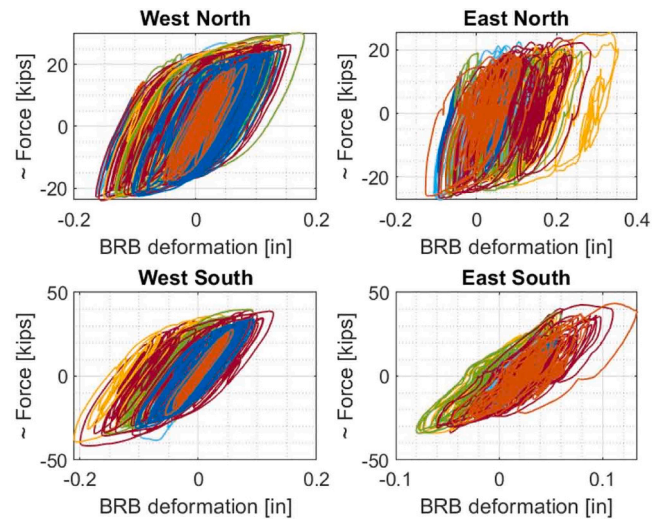


Fig. 9. BRB hysteretic loops for the steps 1–62. Spectral matched motions scaled up to 100 %.

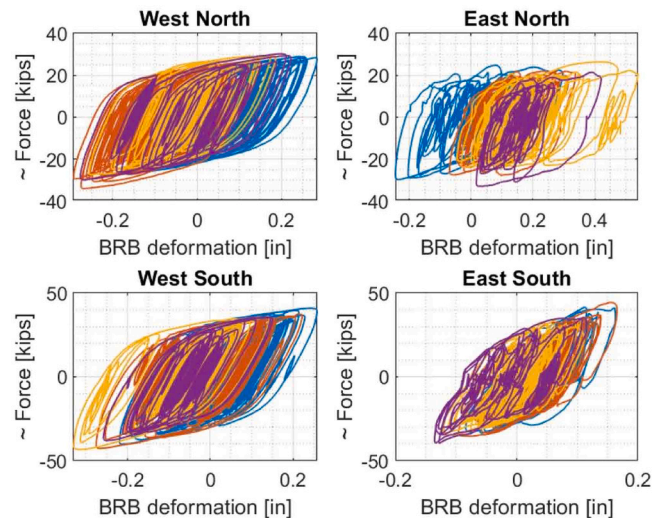


Fig. 10. BRB hysteretic loops for the steps 63–72. Spectral matched motions scaled up to 125 %.

calculate ductility, it was considered that all the BRB deformation was provided by the yielding core. The resulting apparent ductility demands for each BRB and motion at 100 % or larger are listed in Table 3. It was observed that all BRBs developed ductilities of more than 10 without failure, and both BRBs connected to the north girder (i.e., the weaker BRBs) developed ductilities of more than 20 without failure. This confirms that designing BRBs to reach mean ductilities of 10 is possible, and that in extreme cases these BRBs can reach a maximum ductility equal to 20 without failure.

The BRB residual deformations are shown in Fig. 8. Figure shows that the magnitude of this residual deformation varies randomly. The residual deformation varies from one motion to the other and fluctuates from $-0.25''$ to $+0.25''$ until failure. If only data from the motions that have been tested at a scale equal to or larger than 100 % are used, the maximum of the geomean for each BRB of the absolute residual deformation is $0.06''$. By coincidence, the same value was obtained if the apparent residual deformation is used (except that the maximum geomean residual displacement is in a different BRB). Such a value is approximately equal to the average BRB yield deformation, validating the idea that residual displacements should not be a significant issue for

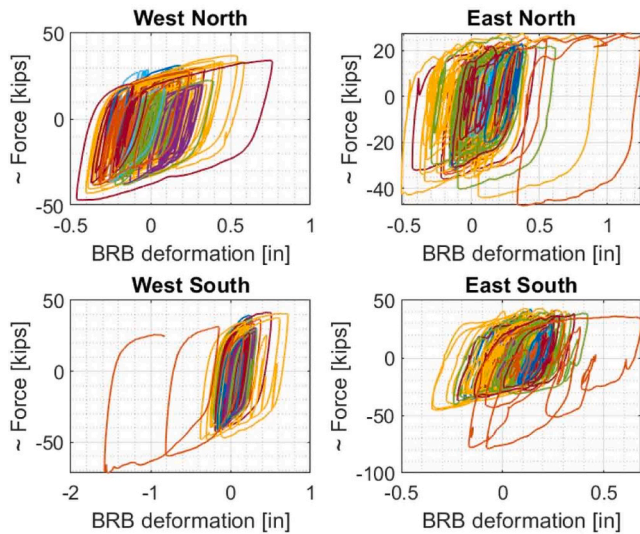


Fig. 11. BRB hysteretic loops for the steps 73–139.

this resilient bridge concept.

6.2. Forces in BRB

The forces were approximated from strain gauges data. Only in the west south BRB, the strains were directly converted into forces using the factor obtained from a calibration process developed as part of this project (which consisted of, before shake table testing, hanging a known weight from one end of the BRB while the other BRB end is hanging from a crane and reading the corresponding strain gauge values), without additional modifications. In the other BRBs, the factors were obtained by adjusting the first tension yielding force from the hysteretic curve to the expected yielding force and adjusting the BRB forces to forces calculated with data from accelerometers. The resultant hysteretic loops are shown in Figs. 9–11.

Note that in Fig. 11, in the east south BRB, the compressive force increases abruptly for Step 134. This increase was observed after the failure of the east north BRB and before impacts to the lateral restraint, and was probably due to the increase bending demand in one of the BRB end plates. Therefore, the compressive forces in this cycle were included in the figure but were not considered in statistics (e.g., calculations of mean results) since they are not considered to be representative of the actual BRB behavior. Comparing forces calculated from the accelerometers data and the approximated forces in BRB, it is estimated that the impact force in the lateral restraint was approximately 30 kips.

6.3. Fatigue

The low cycle fatigue demand calculated using methodology proposed by Li et al. [16] and assuming conservatively that all the deformation was provided by the yielding core are shown in Table 3 for each step. During the spectral matched motions at 100 % (step 62), the fatigue index in all BRBs is less than or equal to 3 % for each individual earthquake. During the steps where extreme motions were used, the maximum fatigue induced by a single earthquake without failure of a BRB was 18 % (with values generally being smaller than that for the other ground motions). In this worst-case earthquake, one BRB would need more than five repetitions of this extreme motion to fail. When the apparent core ductility demand was less than 10, the largest fatigue index was 6 %; for ductilities less than 20, the largest fatigue index was 17 %; for ductilities less than 29, the largest fatigue index was 18 %. This shows BRBs are able to resist multiple severe earthquakes and consequently makes replacement of the BRB following an earthquake

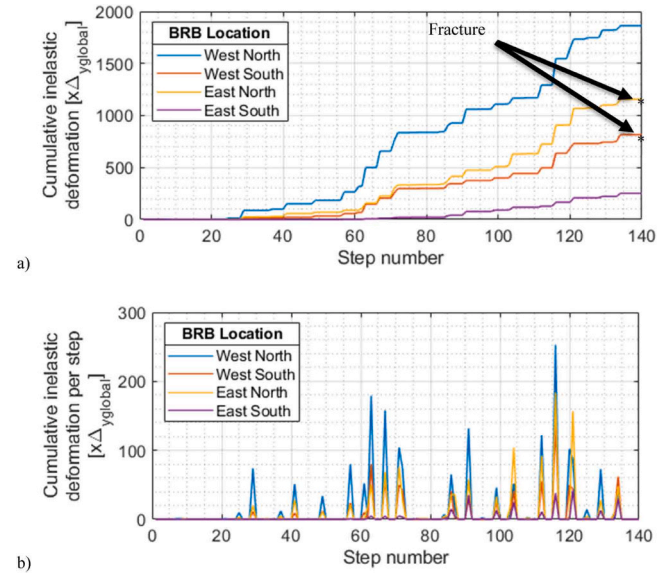


Fig. 12. Cumulative inelastic deformation: a) Cumulative deformation until the end of the test; b) Cumulative deformation in each step.

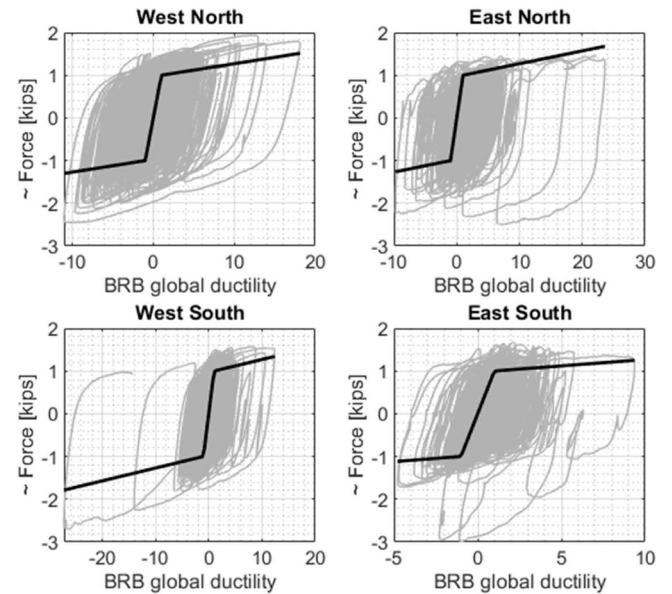


Fig. 13. Numerical backbone curve vs experimental force-deformation hysteretic loops.

unlikely, which meets the resiliency objective of the proposed system for the proposed upper limit ductility demand of 20.

6.4. BRB cumulative inelastic deformation

The cumulative inelastic deformation for each step and for each BRB was calculated as the hysteretic energy of the BRB represented by an elastic perfectly plastic model and normalized by the nominal yield strength times the global yield deformation. Fig. 12 shows the cumulative inelastic deformation for all the test (values are listed in Table 3) and for each step. Through the test program, all BRBs were able to undergo cumulative inelastic demands of more than 200 times the global yield deformation, thus exceeding the requirement to qualify BRBs according to AISC [3]. Furthermore, in all seismic steps except Step 116 with the Mexican record, all individual motions demanded a cumulative inelastic deformation of less than 200 $\Delta_{yglobal}$. For all spectrally matched

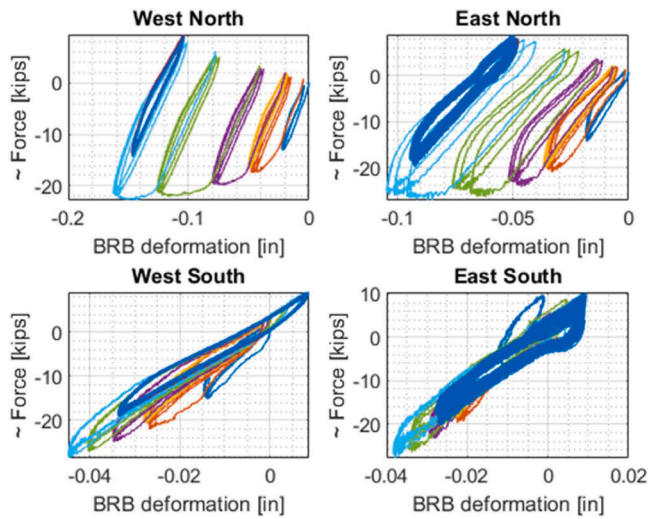


Fig. 14. Hysteretic loops for temperature sequence, first attempt, steps 4–11.

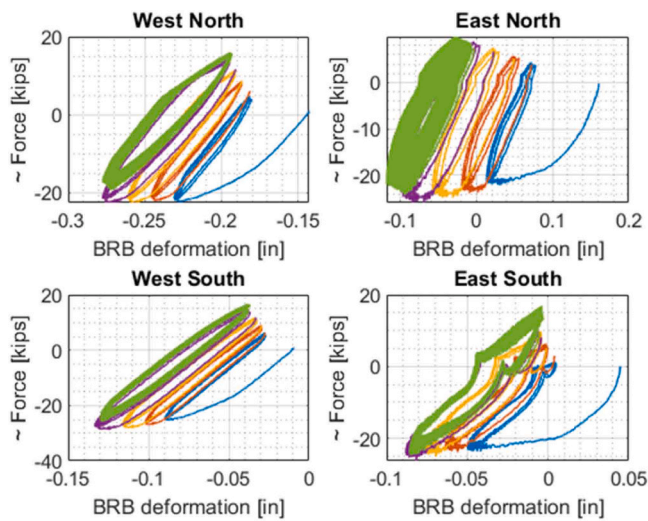


Fig. 15. Hysteretic loops for temperature sequence, second attempt, steps 76–80.

motions (Steps 1 to 62), the maximum cumulative inelastic deformation demand for a single motion was less than $80 \Delta_{yglobal}$.

6.5. Comparison with the backbone curve used in the numerical model

Fig. 13 compares the experimental BRB hysteretic loops with the backbone curve used in the numerical model. In general, the backbone curve predicts smaller yielding than observed in the experiment. This could explain in part why demands in BRBs are smaller than demands from NL-RHA.

6.6. Temperature

The temperature protocol was adjusted during testing. The hysteretic loop of the first attempt is shown in Fig. 14. The amplitude of deformation demand for the 75 cycles in BRBs was smaller than expected, reaching 0.040" instead of 0.089". Therefore, temperature protocol was repeated after spectral matched motions. The hysteretic loop of the second attempt is shown in Fig. 15. The amplitude of deformation demand for the 75 cycles in BRBs in the second attempt was 0.086", 3% smaller than expected. Considering that it was intended conservatively

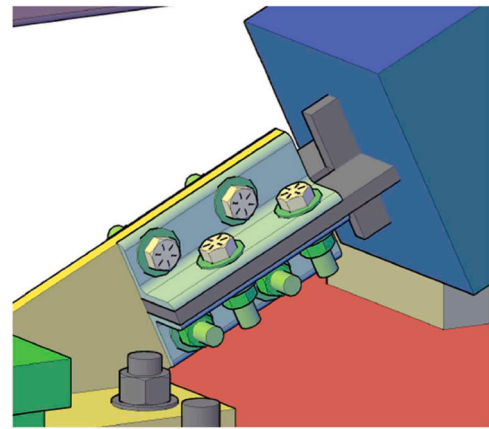


Fig. 16. Connection sketch.

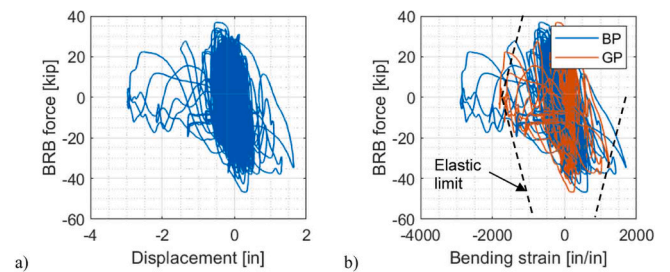


Fig. 17. Demands in gusset plates for the west north BRB compared with force in the BRB: a) displacement, b) bending strain. BP = connection to the foundation, GP = connection to the deck.

that all the temperature deformation would be taken by the BRB, neglecting the deformation can could also be taken by other elements, the 3% difference is not significant. From the figure for the second attempt, it is observed that the plastic deformation due to temperature is taken by the four BRBs since the west and the east pair of BRBs have the same total strength. The total induced fatigue for the WN, WS, EN and ES BRB were 1.10, 1.49, 1.65, and 0.83, which are not significant values.

6.7. Connections

The demands in the connection at each end of the BRBs were analyzed in term of the relative out-of-plane displacements generated at one end of the BRB with respect to the other end, and the bending strains obtained from the strain gauges. All connections considered behaved satisfactorily, but for brevity, example results are presented here for the connection-type shown in Fig. 16. This slip-critical connection has bending demands in the gusset plate and in the BRB end plates. Demands in the gusset plates are shown in Fig. 17. For this BRB, the maximum out-

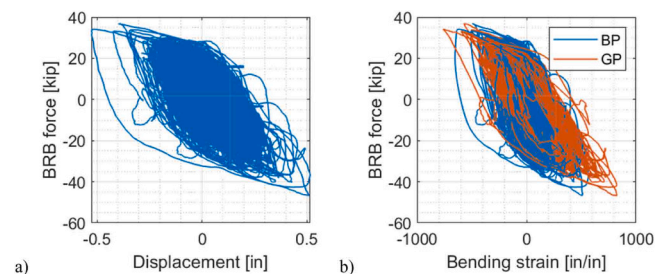


Fig. 18. Vertical demands in BRB endplates for the west north BRB: a) displacement, b) bending strain. BP = connection to the foundation, GP = connection to the deck.

Table 5
Summary of extreme BRB demands for Set 1.

Description	BRB			
	WN	WS	EN	ES
BRB number	7a	7b	8a	8b
Max. deformation [in]	0.76	0.72	1.25	0.68
Min. deformation [in]	-0.46	-1.58	-0.56	-0.35
Max def. amplitude [in]	1.22	2.30	1.81	1.03
Max core strain [%]	3.2	3.0	5.1	2.8
Min core strain [%]	-1.9	-6.7	-2.3	-1.4
Amplitude core strain [%]	5.16	9.73	7.33	4.17
Expected core yielding strain [%]	0.13	0.18	0.13	0.18
Normalized amplitude by core yielding strain	39	53	56	23
Cumulative inelastic deformation	1863	815	1156	252
~ Max. force (Tension) [kip]	36.9	41.4	27.7	44.3
~ Max. force (Compression) [kip]	46.8	71.6	47.6	45.3
ω	1.94	1.57	1.05	2.33
$\omega\beta$	2.46	2.71	1.80	2.38
Final status	—	Failed	Failed	—

* WN = West north BRB, WS = West south BRB, EN = East north BRB, ES = East south BRB

of-plane displacement was 2.91". Assuming that the rotation of the bridge and concrete block are negligible, and knowing that the distance between rotation point is 70.88", the connection underwent an out-of-plane rotation of 0.04 radians (2.35 degrees). The maximum displacement when the BRB yielded in compression is 1.67", equivalent to a rotation of 0.0236 radians (1.35 degrees). In Fig. 17b, dashed lines represent the gusset plate yielding strain at bending considering that axial force is uniformly distributed in the gusset plate at the measuring point (the material yielding strain is 1700 $\mu\text{in/in}$). The figure shows that the bending strain in the gusset plates reached the yielding several times, and at least only one time while the BRB was in compression.

For the bending demand in the BRB endplate, Fig. 18 compares the displacement and bending strain in gussets with the force in the BRB. The maximum vertical displacement was 0.52", which, for a distance between rotation points of 56", corresponds to a rotation of 0.0093 radians (0.53 degrees). The maximum displacement while the BRB is yielding in compression was 0.51", equivalent to 0.0091 rad (0.52 degrees).

6.8. Summary of BRB demands

The maximum BRB demands obtained during the experiment have

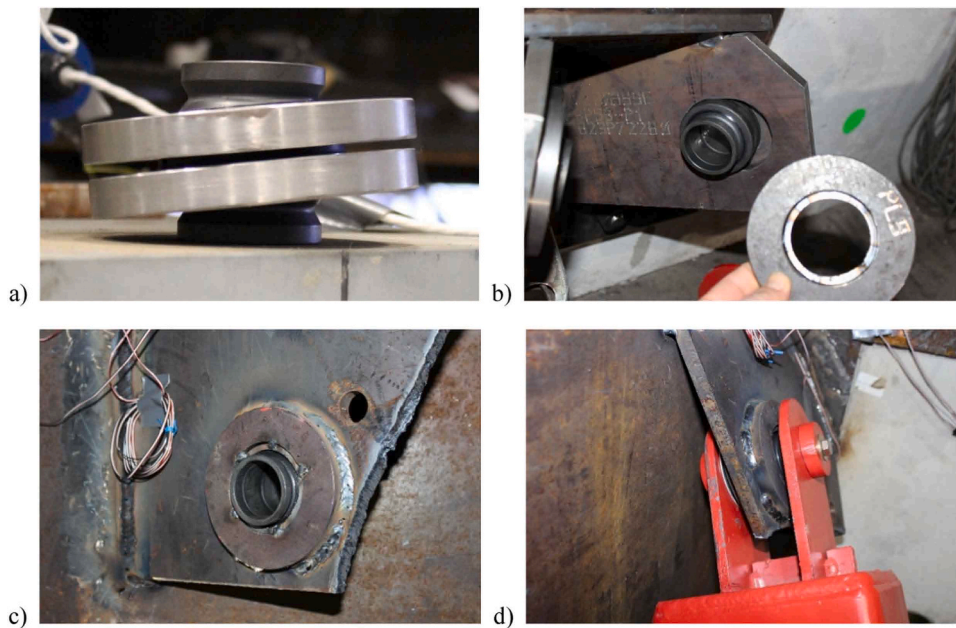


Fig. 19. Photos of BRB connection for the second set of BRBs: a) spherical bearing with washer plates; b) bearing installed in the gusset plate close to the west foundation; c) final position view of the bearing installed in the gusset plate welded to the girder, and; d) BRB installed in the bearing.

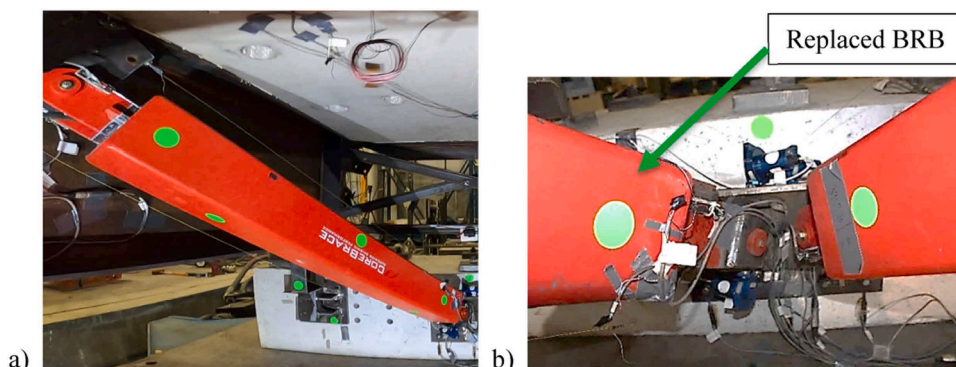


Fig. 20. West South BRB: a) failure of BRB 9b-3, b) replaced by BRB 8b.

been summarized in Table 5. Based on the results from the preliminary axial test of the BRB used for the internal design of all BRBs, the BRB yielding core strains were expected to be in the range of $\pm 3.2\%$ before failure, corresponding to a strain amplitude of 6.4%. However, the BRBs in the specimen subjected to shake table testing performed better, reaching strain amplitudes between 7.3% to 9.7% before failure.

7. Test results for BRBs for Set 2

For the BRBs Set 2, as mentioned earlier, all BRBs were produced with the same core plate. The most significant difference with Set 1, however, was that the BRBs end connections in Set 2 had spherical bearings, as shown in Fig. 19. These spherical bearings effectively introduce a “pinned connection” able to provide free rotation in all directions at the ends of the BRBs. Due to the change in BRBs connections (changed to spherical bearings), the yielding core and thus the yield displacement were larger than originally considered, which required to adjust the design parameters scaling factors accordingly.

This second configuration also performed well and similarly to what was presented above (results not presented for brevity), except for the fact that one BRB failed after being subjected to 9 ground motions (namely, the entire set of spectral matched motions representing design demands for BRBs Set 1, two additional ones of those scaled to 125%, and during the fourth ground motion from the set of spectral matched motions for BRBs Set 2) and temperature records. The failed BRB was replaced with one BRB from the first set that had the same yield strength and that did not fail during testing for Set 1, making modifications to its ends so it could be used with the spherical bearings, as shown in Fig. 20. Note that the bridge was not lifted and all additional masses remained on top of the bridge while the repair was executed, which shows that in the case of a BRB replacement, the bridge could remain operative (in practice, requiring a few hours of closure at night to prevent vibrations while connecting the new BRBs). After BRB replacement, the test continued until the replaced BRB also failed (after 2 more earthquakes at or above the design level), followed by failure of another BRB (after another earthquake). The test ended after several tries to fail the remaining BRBs without success. Results from the test show similar behavior as observed in with the first set of BRBs. Demands were typically smaller than those expected from numerical analysis; this could be partly attributed to the fact that although connections were designed aiming to avoid gaps, experimental results showed that there was a gap of 0.055” in all connections.

8. Conclusions

The proposed bidirectional diaphragm concept with BRB in a V-configuration was validated to perform as intended for a scaled straight bridge with no skew, using one span simply supported specimen on slider bearings. The specimen was able to support 75 years of temperature thermal expansion, and to subsequently be subjected to multiple earthquakes meeting and exceeding the expected design demands. The specimens were subjected to ground motions having 2 orthogonal horizontal components. As such, the ELF design procedure proposed and used in the design of the specimen was validated during testing of the specimen under seismic motions representing the design level. The BRB ductility demands obtained during the test for excitations at the design level were generally less than the mean target ductility value. Additionally, by using stronger motions than considered in design, it was demonstrated that BRBs can withstand deformation ductility demands larger than 20, which was the expected upper limit of ductility considered in the analytical research.

The BRB connections were able to withstand stable out-of-plane and in-plane rotations while the BRBs reached their yielding strength in compression. It was also confirmed experimentally that the possibility of BRB fracture due to a single earthquake is unlikely. Calculation of the fatigue index of tested BRBs showed that no single earthquake could

induce a fatigue index of more than 50%, which confirms that BRBs would not need replacement after an earthquake. Therefore, these bridges would experience no loss of functionality following an earthquake, resulting in fully resilient bridges that remain in service throughout and after the earthquake.

CRedit authorship contribution statement

Homero Fernando Carrión Cabrera: Writing – original draft, Visualization, Software, Methodology, Investigation, Formal analysis, Data curation, Conceptualization. **Michel Bruneau:** Writing – review & editing, Writing – original draft, Supervision, Resources, Project administration, Investigation, Funding acquisition, Conceptualization.

Declaration of Competing Interest

The authors declare that they have no known competing financial interests or personal relationships that could have appeared to influence the work reported in this paper.

Data availability

Data will be made available on request.

Acknowledgments

This study was sponsored by the California Department of Transportation (Caltrans) under research Contract No. 65A0745. This support is gratefully appreciated. The Fulbright program, USA SENESCYT Ecuador, and the University of Buffalo, are acknowledged for their financial support through a scholarship to Homero Carrion Cabrera. This project also benefited from research conducted in parallel and sponsored by the Transportation Research Board of the National Academies under the TRB-IDEA Program (NCHRP-215). This research was also made possible thanks to the significant donations of material and in-kind donations from the American Institute of Steel Construction, the High Industries Inc. companies (High Steel, High Concrete, and High Transit), CoreBrace LLC, and RJ Watson Inc. However, any opinions, findings, conclusions, and recommendations presented are those of the authors and do not necessarily reflect the views of the sponsors.

References

- [1] AASHTO. AASHTO Guide Specifications for LRFD Seismic Bridge Design (2nd Edition. Revision 2015. ed.). American Association of State Highway and Transportation Officials, Washington, DC, USA; 2011.
- [2] Aiken I, Clark P, Tajirian F, Kasai K, Kimura I, Ko E. Unbonded braces in the United States-Design studies, large-scale testing, and the first building application. *Proc Int Post-SMiRT Conf Semin, Korea Earthq Eng Res Cent 1999*;I:317–37.
- [3] AISC. Seismic provisions for structural steel buildings. ANSI/AISC 341-22. Chicago, IL, USA: American Institute of Steel Construction; 2022.
- [4] Alfawakhiri F, Bruneau M. Local versus global ductility demands in simple bridges. *J Struct Eng* 2001;127(5):554–60. [https://doi.org/10.1061/\(ASCE\)0733-9445\(2001\)127:5\(554\)](https://doi.org/10.1061/(ASCE)0733-9445(2001)127:5(554)).
- [5] Bruneau M, Chang SE, Eguchi RT, Lee GC, O'Rourke TD, Reinhorn AM, et al. A framework to quantitatively assess and enhance the seismic resilience of communities. *Earthq Spectra* 2003;19(4):733–52.
- [6] Carden LP, Itani AM, Buckle IG. Seismic performance of steel girder bridge superstructures with ductile end cross frames and seismic isolators (Technical Report MCEER-08-0002). Multidisciplinary Center for Earthquake Engineering Research; 2008.
- [7] Carrion-Cabrera H, Bruneau M. Longitudinal-direction design of buckling restrained braces implemented to achieve resilient multi-span bridges. *Proc Inst Civ Eng-Bridge Eng* 2022;1–28. <https://doi.org/10.1680/jbren.21.00097>.
- [8] Carrion-Cabrera H, Bruneau M. Seismic Response of Regular Multi-span Bridges having Buckling-Restrained Braces in their Longitudinal Direction. *Eng Struct* 2022;259:114127. <https://doi.org/10.1016/j.engstruct.2022.114127>.
- [9] Carrion-Cabrera H, Bruneau M. Asynchronous shake table testing of seismic resilient multi-span bridges having buckling restrained braces in bidirectional ductile diaphragms. *ASCE J Struct Eng* 2024;150(7). <https://doi.org/10.1061/JSENDH.STENG-1284>.

- [10] Carrion-Cabrera H, Bruneau M. Equivalent lateral force design method for longitudinal buckling restrained braces in bi-directional ductile diaphragms. *ASCE J Struct Eng* 2024;150(3). <https://doi.org/10.1061/JSENDH.STENG-12846>.
- [11] Celik OC, Bruneau M. Seismic behavior of bidirectional-resistant ductile end diaphragms with buckling restrained braces in straight steel bridges. *Eng Struct* 2009;31(2):380–93. <https://doi.org/10.1016/j.engstruct.2008.08.013>.
- [12] CIRES. (2005). *Centro de Instrumentación y Registro Sísmico, México*. Available online at: (<http://www.cires.org.mx/>). Accessed November, 2017.
- [13] CoreBrace; 2021. Available online at: (<https://www.corebrace.com/>). Accessed January, 2020.
- [14] Ingham T, Rodriguez S, Nader M. Nonlinear analysis of the Vincent Thomas Bridge for seismic retrofit. *Comput Struct* 1997;64(5-6):1221–38.
- [15] Kanaji H, Hamada N, Ishibashi T, Amako M, and Oryu T. Design and performance tests of buckling restrained braces for seismic retrofit of a long-span bridge. Panel on wind and seismic effects, 21th US–Japan bridge engineering workshop, Tsukuba, Japan; 2005.
- [16] Li C-H, Vidmar Z, Saxey B, Reynolds M, Uang C-M. A procedure for assessing low-cycle fatigue life of buckling-restrained braces. *J Struct Eng* 2022;148(2): 04021259. [https://doi.org/10.1061/\(ASCE\)ST.1943-541X.0003237](https://doi.org/10.1061/(ASCE)ST.1943-541X.0003237).
- [17] PEER. PEER NGA Database. Pacific Earthquake Engineering Research Center, University of California, Berkeley, California; 2006. Available at (<http://peer.berkeley.edu/nga/>).
- [18] SEISMOSOFT. SeismoArtif. (Version 2021) [Computer Program]; 2021. (<https://seismosoft.com/products/seismoartif/>).
- [19] Singaicho JC, Laurendeau A, Viracucha C, Ruiz M. Observaciones del sismo del 16 de Abril de 2016 de magnitud Mw 7.8, Intensidades y Aceleraciones. Sometido a la Revista Politécnica, Instituto Geofísico – Escuela Politécnica Nacional; 2016. Available online at: (<https://www.igepep.edu.ec/servicios/noticias/1324-inf-orme-sismico-especial-n-18-2016>). Accessed June, 2020.
- [20] Wei X, Bruneau M. Buckling restrained braces applications for superstructure and substructure protection in bridges (Technical Report MCEER-16-0009). Multidisciplinary Center for Earthquake Engineering Research; 2016.
- [21] Wei X, Bruneau M. Experimental investigation of buckling restrained braces for bridge bidirectional ductile end diaphragms. *J Struct Eng* 2018;144(6):04018048. [https://doi.org/10.1061/\(ASCE\)ST.1943-541X.0002042](https://doi.org/10.1061/(ASCE)ST.1943-541X.0002042).
- [22] Zahrai SM, Bruneau M. Ductile end-diaphragms for seismic retrofit of slab-on-girder steel bridges. *J Struct Eng* 1999;125(1):71–80. [https://doi.org/10.1061/\(ASCE\)0733-9445\(1999\)125:1\(71\)](https://doi.org/10.1061/(ASCE)0733-9445(1999)125:1(71)).